

Magnetic Properties of Coupled Co/Mo/Co Structures Tailored by Ion Irradiation

Andrzej Wawro,^{1,*} Zbigniew Kurant,² Marcin Jakubowski,¹ Maria Tekielak,²
Aleksiej Pietruczik,¹ Roman Böttger,³ and Andrzej Maziewski²

¹*Institute of Physics, Polish Academy of Sciences, Aleja Lotników 32/46, PL-02668 Warsaw, Poland*

²*Faculty of Physics, University of Białystok, ulica Ciołkowskiego 1L, 15-425 Białystok, Poland*

³*Institute of Ion Beam Physics and Materials Research, Helmholtz-Zentrum Dresden-Rossendorf, Bautzner Landstrasse 400, 01328 Dresden, Germany*

 (Received 12 May 2017; revised manuscript received 13 October 2017; published 26 January 2018)

Modifications of the magnetic properties of Co/Mo/Co films activated by irradiation with 30-keV Ar and 17-keV Ne ion beams are investigated and compared with the influence of 35-keV Ga ions. This system is magnetized in the sample plane and exhibits a twofold anisotropy. The interlayer coupling of magnetization in as-deposited structures is parallel except for the Mo spacer thickness range between 0.5 and 1.0 nm, where the magnetization of the Co layers is antiparallel oriented. The coupling changes and gradually reduced strength of the ferromagnetic properties are compared for all ion types and discussed as a function of the Mo spacer thickness and the ion fluence. The structural evolution of the studied films with increasing fluence determined from TRIDYN simulations is discussed in relation to the observed magnetic changes. We also propose various types of magnonic crystals that can be fabricated by exploiting the results presented in this work.

DOI: [10.1103/PhysRevApplied.9.014029](https://doi.org/10.1103/PhysRevApplied.9.014029)

I. INTRODUCTION

The functionality of layered magnetic structures with coupling oriented in the film plane [1,2] or in the perpendicular direction [3] that essentially influences magnetoresistance [4,5] is confined by the inherent nature of Rudermann-Kittel-Kasuya-Yosida or dipolar interactions. The configuration of spins is constrained to collinear or perpendicular alignments in magnetic layers. Numerous investigations have been carried out to modify the magnetic properties of such structures to enhance their functionality. The strength of perpendicular magnetic anisotropy (PMA) was tuned by a type of overlayer [6] or by inserting an extra ultrathin layer near the interfaces [7]. Other efforts to modify anisotropy have been undertaken with the use of ion and laser irradiation. Irreversible magnetization switching from perpendicular to in-plane alignment [8] and in the opposite direction [9] was induced by ion irradiation. An ion beam has modified also antiferromagnetic coupling [10–12], magnetic dumping [13], and tuned PMA [14]. While in most layered structures, ion irradiation suppresses ferromagnetic properties, in the FeAl system, ferromagnetism is induced through the creation of chemical disorder [15]. Magnetic patterning by ion irradiation is widely reviewed in Ref. [16]. Similar effects leading to PMA enhancement were obtained through irradiation with laser

pulses [17–19]. The coupled structures with tuned perpendicular magnetizations [20] and new magnetic ordering [21] were investigated as well. The properties of coupled structures were enhanced by a combination of components exhibiting in-plane and out-of-plane magnetizations [22,23]. Tunable tilted magnetic anisotropy was obtained through modifying their exchange spring behavior by inserting appropriate spacers [24]. Doping of the interfaces with paramagnetic impurities (so-called “loose spins”) was another approach in tailoring the coupled systems [25–28]. The observed orthogonal alignment of magnetization in the component layers was explained theoretically [29] by biquadratic contribution to the coupling strength. Recently, it was suggested that the properties of individual layers can be freely adjusted during the deposition process of individual layers by oblique incidence deposition [30]. This approach may enhance considerably the functionality of magnetoresistive devices for spintronic applications.

Relatively few papers were devoted to the Co-Mo system, although potentially it seems to be attractive for various applications. It exhibits some useful properties in catalysis [31,32]. This system is also expected to be a good material for high-density magnetic recording media and potential applications in magnetic sensors due to enhanced magnetic anisotropy energy, magnetization saturation, and low coercivity [33]. Most investigations have focused on phase evolution correlating with magnetic properties. Amorphization of Co-Mo systems was studied under

*Corresponding author.
wawro@ifpan.edu.pl

thermal annealing and ion irradiation [34] or as an effect of the ion-beam-assisted deposition process [35]. Evolution from bcc ferromagnetic to amorphous superparamagnetic films was observed for two-monolayer-thick Co films [36]. Domination of the hcp or bcc Co arrangement depended on the relations between the thickness of the component layers d_{Mo} and d_{Co} [37]. The concept of a dead layer was connected with antiferromagnetic coupling at the interface, lowering the Curie temperature or structure deformation [38]. On the other hand, the fcc Co phase was identified in Co films 2 nm thick [39]. It changed to hcp alignment with a d_{Co} increase. A decrease of magnetization saturation in the thinnest component layers was attributed to nonmagnetic ϵ -phase Co_7Mo_6 that developed at the interface. Numerous sequential phase crossovers from amorphous in an as-deposited 58/42 structure to paramagnetic and further to hcp ferromagnetic, fcc ferromagnetic and the intermetallic compound Co_7Mo_6 were inferred with an annealing temperature increase [40]. Several theoretical works have predicted the existence of possible Co-Mo phases. Magnetically induced phase separation with Curie temperature was deduced from thermodynamic simulations [33]. Gibbs free-energy calculations showed stability of bcc, hcp, and amorphous phases [35]. *Ab initio* methods applied for the total energy confirmed the equilibrium σ phase [41] and nonequilibrium structures—hcp located near Co_3Mo and A15 near CoMo_3 [42].

Coupling effects in the Co/Mo multilayers were reported merely in a few works. Parkin showed that oscillatory exchange coupling of the Co layers deduced from the oscillatory behavior of the saturation field was a general phenomenon among the transition-metal spacers [43]. The strength of the coupling increased both with d -shell occupation and along each column in the table of elements. A well-distinguished coupling with induced in-plane anisotropy was reported in sputtered structures [44]. The theoretical analysis of electronic structure and crystallographic orientation influence on the Co-layer coupling were carried out for the various types of transition-metal spacers, including Mo [45].

In this work, the influence of 17-keV Ne and 30-keV Ar ion irradiation on magnetic properties in Co/Mo/Co-layered structures is partially compared with 35-keV Ga ions' influence and discussed as a function of the Mo spacer thickness d_{Mo} and the ion fluence F . As-deposited samples are magnetized in the plane and exhibit twofold anisotropy. Moreover, in the d_{Mo} range between 0.5 and 1.0 nm, the interlayer coupling of magnetization is antiparallel. We discuss the change of the coupling character and the gradual suppression of the ferromagnetic properties due to progressive intermixing with increasing ion fluence. The observed magnetic modifications are explained by structural evolution inferred from TRIDYN simulations [46]. These investigations are an initial step toward fabrication of magnetically patterned materials in the nanometer scale

with the use of a focused-ion-beam (FIB) technique. Such periodical structures proposed at the end of this work can find potential applications in optospintronics as, e.g., magnonic crystals.

II. EXPERIMENT

The investigated epitaxial-layered structures are deposited in a molecular-beam-epitaxy system (Prevac) onto sapphire substrates $10 \times 10 \text{ mm}^2$ cut along an (11-20) plane, optimal for epitaxial growth. All component materials are evaporated from the electron guns with rates at the level of 0.05 nm/s measured by quartz balance and a Hiden XBS system. Vanadium buffer deposited at room temperature and annealed at 500 °C for 3 h exhibits compatible crystalline structure to the substrate and secures a high quality of the grown sample. Moreover, the energy of the L edge differs from the remaining components, which is crucial for x-ray circular dichroism measurements not reported in this work. The remaining part of the samples is deposited at room temperature. The wedge profile of the spacer is obtained with a linear shutter moving during the deposition process. The crystalline structure is monitored *in situ* by reflection high-energy electron diffraction. Ion irradiation is performed using the 40-kV ion implanter (Danfysik A/S, model 1050). Prior to the irradiation process, its parameters are selected based on the simulations performed using the TRIDYN package anticipating structural modifications. Three ion types are chosen for irradiation. Ar and Ne are heavier noble gas ions and more effective in modifications than frequently reported He. They are also inert to the sample lattice. Moreover, Ga and Ne are available in commercial FIB tools. To achieve a fluence gradient on the sample, an additional linear Si shutter is placed directly in front of the sample. The shutter is moved in steps of 100 μm . After each shutter movement, the exposed sample is irradiated to a defined fluence. A typical ion-beam spot has a nearly circular shape and a diameter of 5–15 mm depending on the ion energy, ion flux, and focus settings. The implanted ion fluence is measured using four-corner Faraday cups directly behind the sample plane, which are connected to a calibrated charge integrator. The ion-beam current is varied in a range between 6 and 26 nA/cm² to achieve an appropriate irradiation fluence. The sample temperature is not measured during ion irradiation. However, it is known from the earlier experiments that the sample temperature for similar ion-beam parameters (30 keV, 200 nA/cm²) and sample size stays below 40 °C. The applied fluence range is limited by the beam stability from the low end and by expected substantial mixing from the high end. The appropriate setting of the shutter speed and the Mo deposition rate (Mo wedge growth) as well as the applied ion fluence (irradiation) allows us to obtain the samples with the desired gradient parameters. Other details of the irradiation are provided in a further part of this work. The gradients of the Mo spacer thickness and the irradiation fluence are

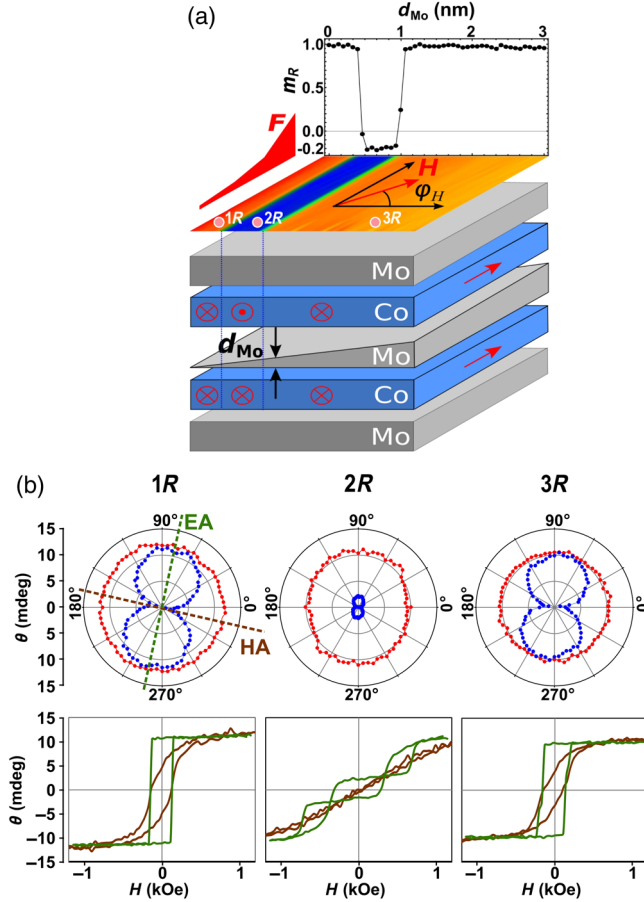


FIG. 1. (a) Schematic representation of the sample configuration, irradiation fluence profile (red wedge), and the orientation of the applied field while the angular dependences of θ_{max} and θ_{rem} are measured. Color map above the sample structure illustrates magnetization alignment in the nonirradiated sample. Top: Normalized remanent magnetization (m_R) as a function of the Mo spacer thickness d_{Mo} . (b) Top row: Angular dependence of θ_{max} (red) and θ_{rem} (blue) with marked easy (EA) and hard (HA) in-plane anisotropy axes. Bottom row: LMOKE hysteresis loops measured in the field applied along the EA (green) and HA (brown) in three characteristic zone spots (1R, 2R, 3R) of the pristine sample.

mutually orthogonal. In this way, matrixlike samples with spatially changing properties as a function of (d_{Mo} , F) are obtained. The magnetic properties are investigated locally in a magnetometer exploiting the magneto-optical Kerr effect (MOKE). Because of the low total structure thickness, the signal is achieved from the whole sample depth, however, with slightly different weights. It is averaged over the area covered with the laser spot, 0.3 mm in diameter, larger than the shutter step in the ion-irradiation process. Because of the in-plane magnetization alignment, the measurements are carried out in a longitudinal configuration (LMOKE). In this setup, the magnetic field can be applied in any direction in the sample plane. The magneto-optical measurements are performed at room temperature.

III. RESULTS

A schematic sample configuration is shown in Fig. 1(a). Two Co(0001) 3-nm-thick layers separated with a Mo(110) spacer shaped as a wedge $0 < d_{\text{Mo}} < 3$ nm constitute a core of the investigated samples. This trilayer is wrapped from the top and bottom with two Mo(110) layers 1 nm thick. Moreover, this structure is deposited on a 2.5-nm V(110) buffer and capped with a 3-nm V(110) overlayer (these layers are not shown for simplicity). Various aspects of the Co-layer growth on the Mo surface are reported in Refs. [47–49]. The crystalline structure, induced strains, and interface quality in the samples fabricated under the identical conditions as investigated here are discussed in detail in Ref. [50]. Magnetization of the as-deposited samples is oriented in the plane with clearly distinguished twofold anisotropy determining the easy (EA) and hard (HA) anisotropy axes. The magnetic anisotropy is a consequence of anisotropic strains induced at the interfaces due to structural and lattice parameter mismatches between the Mo(110) and Co(0001) planes. Moreover, this system exhibits interlayer coupling depending on the Mo spacer thickness. In the range $0.5 \text{ nm} < d_{\text{Mo}} < 1.0 \text{ nm}$, the coupling is antiparallel (AP); i.e., the magnetization of the Co layers is oriented mutually in opposite directions along the EA. Beyond this range, both for the thinner and thicker Mo spacer, the magnetization is aligned parallel (P), again, along the EA. The AP alignment of the magnetization is illustrated by the stripe in deep blue on the map (representative of the nonirradiated sample) and is visible as a well in the normalized remanent magnetization dependence on the Mo spacer thickness in Fig. 1(a). The angular dependence of Kerr rotation at maximum applied field of

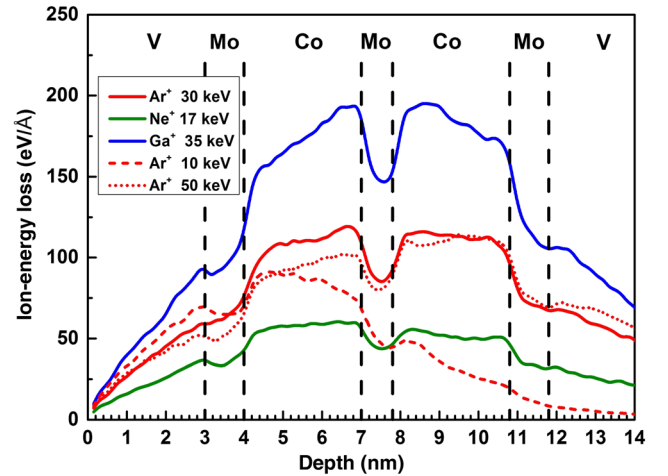


FIG. 2. Ion-energy-loss profiles along the sample depth. Solid lines correspond to the ions and energies applied in the experiment. The dashed and dot lines, as comparison, show the profiles for Ar ions with energies of 10 and 50 keV, respectively. The dashed vertical lines indicate the interfaces in the as-deposited sample.

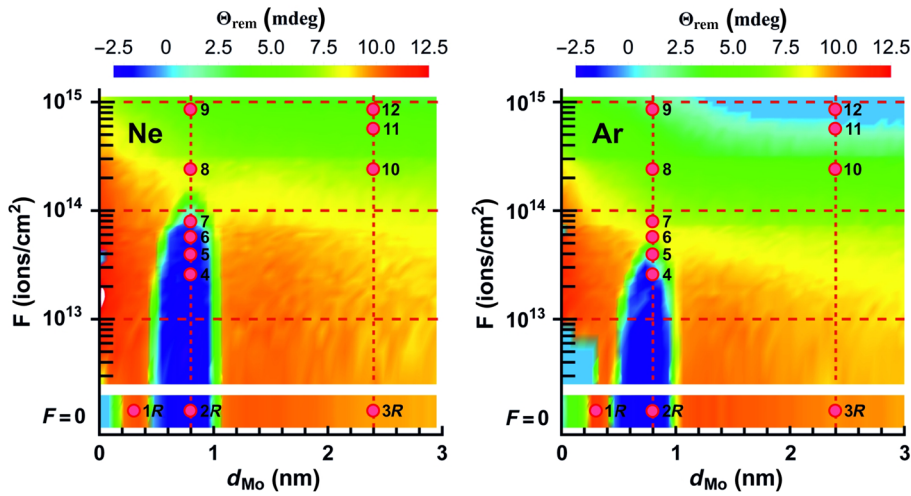


FIG. 3. Maps of $\theta_{\text{rem}}(d_{\text{Mo}}, F)$ measured along the EA after irradiation with 17-keV Ne and 30-keV Ar ions. The bottom separated part of the map represents the reference ($F = 0$) sample. The vertical dashed lines correspond to two characteristic Mo spacer thicknesses $d_{\text{Mo}} = 0.8$ and 2.4 nm discussed in the text. The measurement spots of the magnetic properties shown in Figs. 1, 4, and 5 are marked with the numbered circles. The bright blue areas in the left part of the maps are the shadows (no deposited material; magnetic signal equal to zero) from the sample mounting clamps in the deposition process.

1.2 kOe (θ_{max}), and Kerr rotation at remanence (θ_{rem}) as well as the hysteresis loops measured in the field along the easy and hard anisotropy axes exhibit details of the sample magnetization [Fig. 1(b)]. The orientation of θ_{rem} angular dependence determines the EA ($\theta_{\text{rem}} = \theta_{\text{max}}$). The hard axis is orthogonal to the EA. The rectangular hysteresis loops 1R and 3R both for the smaller and bigger Mo spacer thicknesses are typical of the magnetization aligned parallel along the EA. The magnetization of both Co layers switches simultaneously by 180° . The orientation of the EA is the same for both *P*-coupled zones. For AP coupling, a well-distinguished plateau is visible in the loop 2R measured along the EA. The range of the plateau determines the coupling strength reaching 0.8 kOe. The shift of lines in the vertical direction is caused by different contributions from both Co layers to the LMOKE signal. Tilted $M(H)$ dependence measured in the field applied

along the HA is typical of magnetization rotation from the EA toward the HA [loops 1R–3R marked in brown in Fig. 1(b)]. The closed loop, linear in shape and evidently higher saturation field (2R) is a consequence of additional AP coupling, which makes the magnetization stiffer along the EA.

A scheme of ion irradiation is presented in Fig. 1(a). A nonirradiated stripe of the sample approximately 1.5 mm wide extending along the d_{Mo} gradient serves as a reference as-deposited sample. The selected kinetic energy of ions (17-keV Ne, 30-keV Ar, and 35-keV Ga) is chosen to deposit a maximum energy to the sample in the vicinity of the Mo spacer. At these energies, the nuclear stopping dominates; however, the electronic stopping is not negligible. According to such an assumption, structural changes induced by irradiation are expected to appear mainly at the interfaces between the Mo spacer and adjacent Co layers.

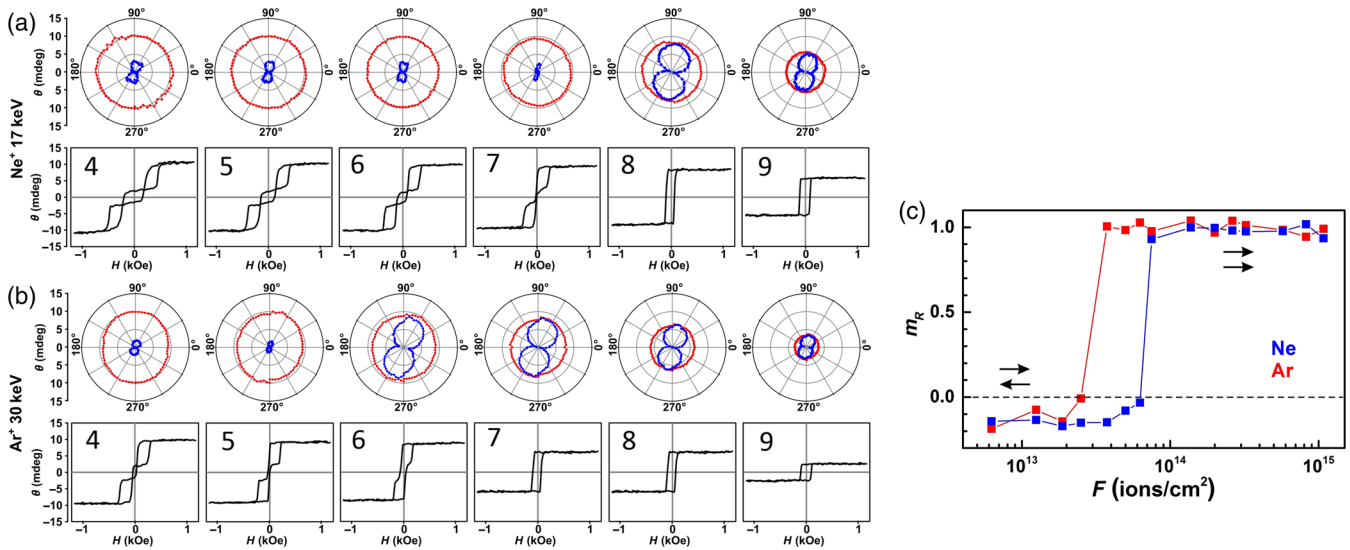


FIG. 4. Evolution with F of the θ_{max} (red) and θ_{rem} (blue) angular dependence and the hysteresis loops measured along the EA for $d_{\text{Mo}} = 0.8$ nm for Ne (a) and Ar (b) ions (positions of the measurement spots are indicated on the maps in Fig. 3). (c) m_R dependence on F for both ion types. Magnetization alignment of the Co layers is marked with arrows.

Figure 2 depicts the energy-loss distribution for different ion types. All profiles are symmetrical around the Mo spacer. The change of ion energy results in strong asymmetry as shown for Ar ions. The applied fluence ranging between 2.50×10^{12} ions/cm² and 1.08×10^{15} ions/cm² is the same for all ions. Three fluence gradients are applied to irradiate the sample area in an optimum way. In a further part of this work, we compare the irradiation effects of Ar and Ne ions with Ga ions [51].

Figure 3 shows two maps of $\theta_{\text{rem}}(d_{\text{Mo}}, F)$ measured along the EA for Ne and Ar ions. These maps cover the whole sample surface. A similar map for Ga ions is discussed elsewhere [51]. A dark blue area extending in the nonirradiated part of the samples and the lower- F range corresponds to the AP magnetization alignment. In the reference part, its borders are sharp and parallel. As the fluence increases, this area becomes slightly narrower, particularly for Ar ions, with the left border shifting toward bigger d_{Mo} . A fluence responsible for transition from AP to P alignment evidently depends on the ion type. For Ne, it is substantially higher than for Ar, as the energies of Ne and Ar ions differ by a factor of 2, and is equal to 7.75×10^{13} ions/cm² and 3.75×10^{13} ions/cm², respectively. The second bright blue area in the high-fluence zone, visible merely in the map for Ar ions, reflects θ_{rem} suppression. In the bigger- d_{Mo} range, its border runs along a constant fluence value ($F = 6.25 \times 10^{14}$ ions/cm²). With a d_{Mo} decrease, the border turns to the higher F . A gradual θ_{rem} decrease with F in the remaining part of the samples exhibiting parallel alignment of magnetization is a common feature of both maps.

More detailed insight into the magnetic properties' modifications can be gained from the hysteresis loops and θ_{rem} and θ_{max} dependences presented in Figs. 4 and 5.

The strength of AP coupling ($d_{\text{Mo}} = 0.8$ nm) gradually decreases from the maximum value in the as-deposited sample state to zero for the fluence forcing crossover to the P coupling [Fig. 4(a), loops 4–7 for Ne ions and Fig. 4(b), loops 4 and 5 for Ar ions]. The rate decrease is lower for the Ne ions as the critical fluence responsible for the crossover is higher. This difference is well distinguished in the m_R (normalized magnetization remanence) dependence on F [Fig. 4(c)]. The abrupt crossover of m_R from low value (AP coupling) to high value (P coupling) occurs for clearly higher fluence of Ne ions in comparison with Ar ions. In the range of P coupling, the hysteresis loops (loops 8 and 9 for Ne ions and 7–9 for Ar ions) take a rectangular shape with the saturation of the Kerr rotation decreasing with the F increase. The sequence of the θ_{rem} angular dependences shows that the direction of the EA is not affected by irradiation. This means that the magnetization at remanence of either antiparallel- or parallel-coupled Co layers is oriented along the same direction. A decrease of the θ_{max} plot diameter with F illustrates a reduced saturation of magnetization.

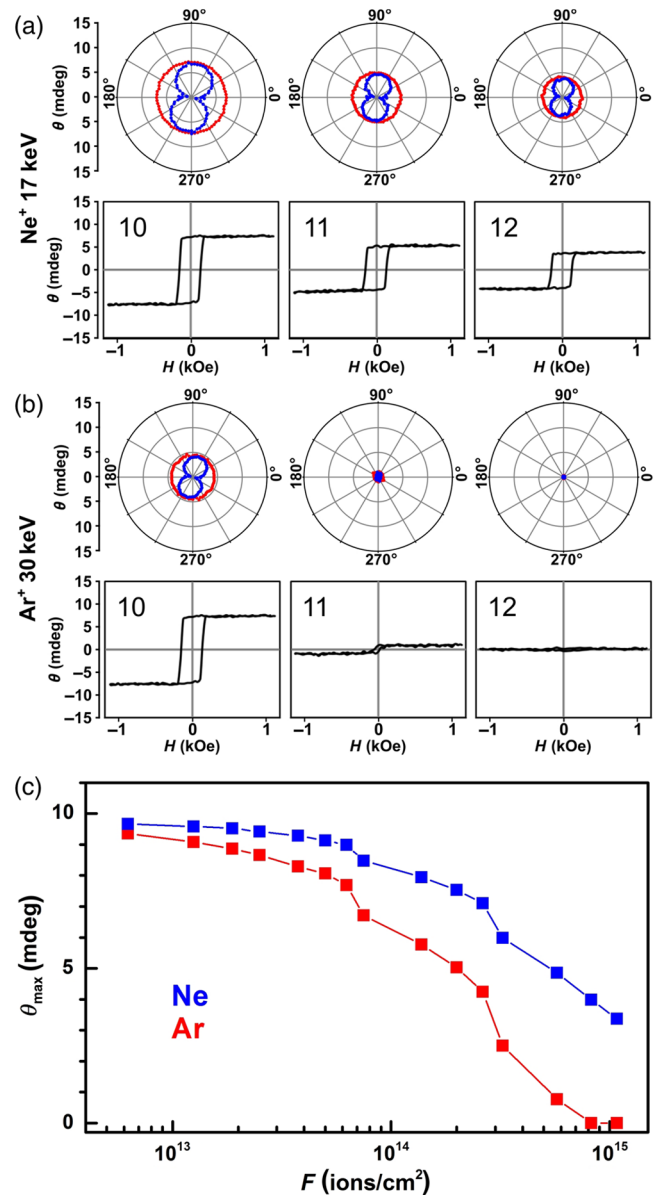


FIG. 5. Evolution with F of the θ_{max} (red) and θ_{rem} (blue) angular dependence and the hysteresis loops measured along the EA for $d_{\text{Mo}} = 2.4$ nm for Ne (a) and Ar (b) ions (positions of the measurement spots are indicated on the maps in Fig. 3). (c) θ_{max} dependence on F for both ion types.

A similar tendency is observed in the range of bigger ($d_{\text{Mo}} = 2.4$ nm) Mo spacer thickness, where the coupling in the as-deposited sample is parallel [Figs. 5(a) and 5(b)]. In the whole F range, the loops are rectangular with a gradually decreasing saturation of the Kerr rotation from the maximum value for the as-deposited sample to zero (for the sample irradiated with Ar) at the border with the blue area at the high- F range (see the θ_{rem} map for Ar ions in Fig. 3). Also in this case, the EA orientation is conserved, regardless of the applied fluence. For the highest Ar beam fluence, a lack of LMOKE signal [spot 12 for Ar in Fig. 5(b)] evidences a full quenching of magnetic

properties. The different efficiencies of both ion types are shown in Fig. 5(c). For the same fluence, θ_{\max} is more strongly suppressed for Ar ions reaching zero value when the magnetization is entirely quenched.

Some common features for both analyzed d_{Mo} thicknesses are observed in the irradiated samples with P alignment of magnetization. At lower fluences, coercivity (H_C) takes a constant value. With further F increase, H_C and the area of the hysteresis loops decrease. The loops retain, however, their rectangular shape up to the highest applied fluences. The observed changes indicate evident suppression of the ferromagnetic properties with the F increase.

It should be emphasized that the θ_{rem} suppressions in both areas marked in blue on the map for Ar ions are of different origin. In the lower- d_{Mo} and $-F$ range, the low value of θ_{rem} arises from antiparallel alignment of nonzero magnetizations, whereas in the high- F range, the magnetization of the sample is entirely suppressed at room temperature.

IV. DISCUSSION

The observed magnetic modifications can be clearly explained by the structural evolution of the layered samples with increasing ion fluence calculated using the TRIDYN package. Although the simulations provide only approximate insight into the sample structure, their results correlate well with the observed alterations of the magnetic properties. Figure 6 depicts four maps of in-depth chemical profiles changing with the fluence for both ion types and two Mo spacer thicknesses equal to 0.8 and 2.4 nm corresponding to AP- and P -magnetization alignment, respectively, in the as-deposited state. The color scale illustrates the concentration distribution of Co atoms. The gray area between the Co layers and outside corresponds to the Mo spacer and the covers, respectively. The buffer and the cap layer made of vanadium are also marked with gray. Mixing at the interface of magnetic layers occurs mostly between the Co and Mo atoms. Similar maps are calculated for the V buffer and cap layers (not shown in this work, as V plays a minor role in magnetic property modification). Because the contribution from the V atoms to the coupling-type change is negligible, and to the quenching of magnetization insignificant, it is limited in the further discussion. Similar maps showing the structural modifications for Ga ions are reported elsewhere [51]. The mixing degree at the interfaces substantially increases with the fluence. The bent upper edge of the maps reflects the surface etching depth by the ion beam. It is lower than 1 nm in all cases in the applied fluence range.

From the maps of the depth chemical composition (Fig. 6), the concentration profiles for the selected applied fluences can be easily extracted. The profiles for two particular fluences—forcing AP- P coupling crossover and

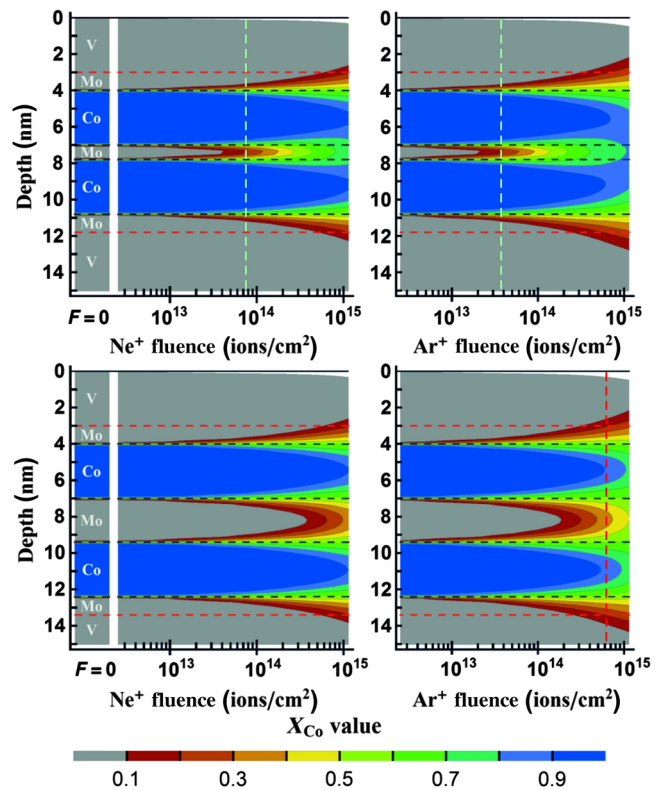


FIG. 6. In-depth chemical profile evolution with F of the irradiated samples for both types of ions (Ne, left column; Ar, right column) and two Mo spacer thicknesses ($d_{\text{Mo}} = 0.8$ nm upper row and $d_{\text{Mo}} = 2.4$ nm bottom row). The separated parts of the maps on the left represent the layered structure of the pristine sample ($F = 0$). The bent upper edges of the maps reflect the surface etching by the ion beam. Horizontal dashed lines indicate the positions of the interfaces in the pristine sample. The vertical bright green dashed lines correspond to F forcing coupling crossover from AP to P , whereas the vertical red dashed line points the fluence suppressing ferromagnetism.

quenching the ferromagnetic properties—are discussed below.

The upper row of Fig. 7 shows the composition profiles of all sample components for the fluences of Ne, Ar, and Ga ions, at which the magnetization alignment is changed from AP to P . At this stage of mixing, the concentration of the Co atoms is lowered only in the vicinity of the interfaces. A part of these atoms is located in the Mo spacer. The coupling crossover occurs when in the middle of the Mo spacer Co atoms reach a level of 20% (indicated by the X_{Co} arrow). For both types of irradiating ions, conformity of these values is highly satisfying, taking into account an approximate character of simulations. The influence of V atoms from the outer covers on the coupling change is negligible. Their concentration drastically drops in the adjacent outer Mo layers and V atoms do not reach the interface between the Co layer and Mo spacer. Also, the concentration of the irradiating atoms along the whole sample depth is negligible.

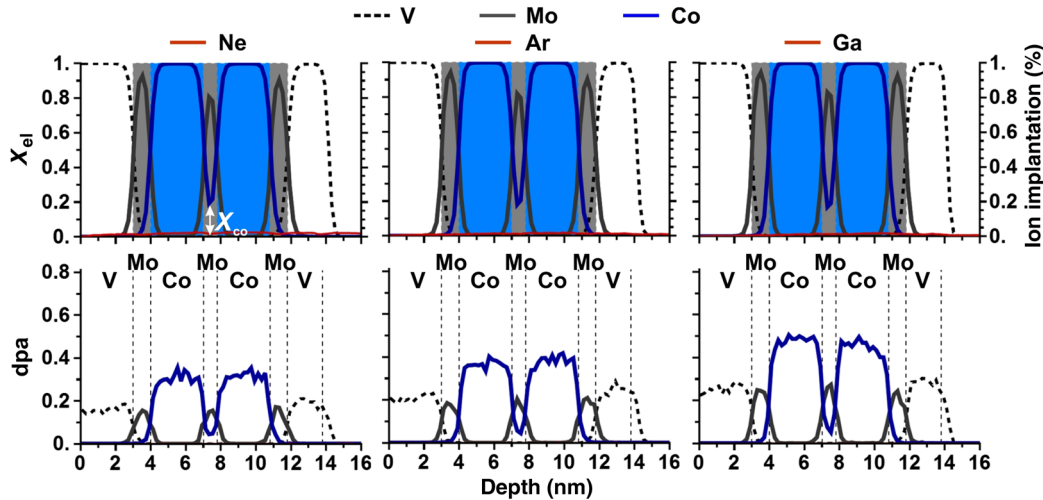


FIG. 7. Upper row: In-depth composition profiles of all constituents (left axis) and implanted ions (right axis) in the samples with $d_{\text{Mo}} = 0.8$ nm at the ion fluences forcing AP-P crossover. The white arrow indicates the Co concentration in the center of the Mo spacer discussed in Fig. 9. Bottom row: dpa profiles.

The displacement per atom (dpa) for the fluence forcing the interlayer coupling change is depicted in the bottom row of Fig. 7. The plots show how many atoms are removed from their sites to make vacancies. Particularly, in the Co layers, nearly every second atom seems to be involved in this process. Its intensity rises from Ne to Ga ions as their energy increases. On the other hand, the twofold in-plane anisotropy and the orientation of the EA are retained even at the highest applied fluences (Fig. 4). This may indicate that the structure of the Co layers and the strains induced by the interfaces are not modified substantially. It is likely that displaced atoms refill the vacancies again, and the actual structure destruction is less severe than expected merely from the dpa calculations.

On this basis, it is not possible to judge which particular mechanism is responsible for the emerging ferromagnetic coupling. The two most possible impacts should be considered: the interface roughness increase that induces magnetostatic interactions and the formation of ferromagnetic bridges (so-called “pinholes”) that connect both Co layers and align their magnetization in parallel by transferred exchange interaction. The alloy effect of Co “loose spins” in the Mo spacer should be taken into account also. However, this model is proposed to explain an orthogonal coupling between the magnetic layers [29].

The in-depth composition profiles of the sample components and irradiating ions for the fluence-quenching ferromagnetic properties in the sample with $d_{\text{Mo}} = 2.4$ nm irradiated with Ar and Ga ions are shown in the upper row of Fig. 8. The irradiation causes mixing of Co and Mo atoms in the whole volume of the core trilayer. The maximum concentration of Co atoms is suppressed in the middle part of the layer below 90%. This concentration substantially decreases in the vicinity of the interfaces. In a boxlike approximation, the mean concentration of Co atoms in the area of the pristine layer reaches a level of approximately 80%. Also, V atoms are spread wider in the sample volume at these fluences, reaching the outer part of

the Co layer. However, the total concentration of Mo is substantially higher there than V, and Co-Mo alloying is probably mostly responsible for the observed ferromagnetism quenching. The implantation of irradiating ions takes the higher level here; nevertheless, it stays much below 1%. A maximal fluence of Ne ions applied in this experiment is still insufficient to suppress the ferromagnetism in Co/Mo/Co structures with $d_{\text{Mo}} = 2.4$ nm.

The bottom row of Fig. 8 shows the dpa at the fluences of Ar and Ga ions that are responsible for ferromagnetic quenching. The lower value is related to much a lower concentration of the respective atoms due to progressed smearing of the layered structure. The arguments explaining the less severe real structural destruction (Fig. 5) than that expected from dpa calculations are the same as used above for the sample with $d_{\text{Mo}} = 0.8$ nm.

The surface etching process should be excluded as a mechanism responsible for ferromagnetism quenching.

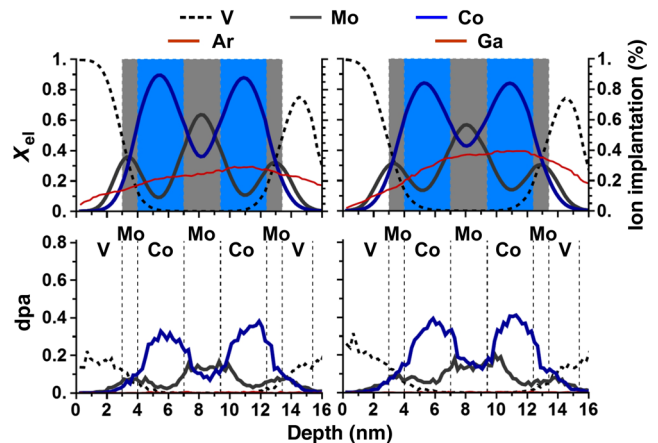


FIG. 8. Upper row: In-depth composition profiles of all constituents (left axis) and implanted ions (right axis) in the samples with $d_{\text{Mo}} = 2.4$ nm at the ion fluences suppressing ferromagnetism. Bottom row: dpa profiles.

The resputtering depth is less than 1 nm; thus, the Co atoms are not removed from the sample even at the highest applied fluence. Therefore, a mixing of the Co layers mainly with Mo atoms from the spacer is a reasonable explanation. It is in good agreement with the irradiation experiment assumption that the maximum of energy transferred from the ion beam to the sample should be deposited in the Mo spacer. Such a justification is supported by the following observations. In the zone of P alignment, the magnetization saturation decreases with the fluence. As the fluence increases, the degree of mixing also increases, which results in a gradual decrease of the magnetic moment per Co atom. At a certain critical value of F , the mixing extent is high enough to suppress the ferromagnetism at room temperature. Also, the border shape between the magnetic and nonmagnetic areas (Fig. 3, Ar ions) correlates well with this explanation. In the range of the thinnest spacer, the number of Mo atoms solved in Co is too low to suppress the magnetic behavior of the sample. As d_{Mo} increases, the alloying degree increases as well and becomes fluence dependent. In this d_{Mo} range, the border is oblique on the map. Above $d_{\text{Mo}} = 1.5$ nm, the crossover does not depend on the fluence, and it is observed for the constant value of approximately $F = 6.25 \times 10^{14}$ ions/cm². Mo atoms are supplied from the source (i.e., from the thicker Mo spacer) in excess of the required number for ferromagnetism suppression in the Co layers.

Our findings deduced from the concentration profiles shown in Fig. 8 are in good agreement with experimental results and theoretical considerations reported by Shan *et al.* [52]. The full suppression of magnetization at room temperature is found for Co concentration of approximately 70% in Co-Mo alloy. Moreover, the mean field model calculations show that the magnetic moment of the alloy is destroyed by only two Mo neighbors surrounding the Co atom. In both bcc structure and close packed, such a surrounding corresponds to a Co concentration equal to 87%. Also, the calculated phase Co-Mo diagram shows that an intermetallic compound is formed with approximately 75% Co content [41]. The observed ferromagnetism quenching may be associated with Curie temperature (T_C) of the samples that reaches the room value.

However, the $T_C(F)$ dependence investigations are out of the scope of this work.

The efficiency of 35-keV Ga ions and 30-keV Ar ions in magnetic property modification is evidently higher than that of 17-keV Ne ions. Although the quantitative differences are clear, the qualitative influence is similar. In other words, a higher fluence of Ne ions is required to obtain the same effects as for Ar or Ga ions. This similarity is illustrated in Fig. 9. Figure 9(a) shows the map of $\theta_{\text{rem}}(d_{\text{Mo}}, F)$ after irradiation with 35-keV Ga ions. All characteristic components are qualitatively similar as in the map for Ar ions (Fig. 3). Moreover, the dependence of normalized remanent magnetization measured along the EA for $d_{\text{Mo}} = 0.8$ nm as a function of the Co concentration in the middle of the Mo spacer (indicated by the arrow in Fig. 7) is analogous. The Co concentration is determined from the chemical profile maps (Fig. 6) for various ion fluences. The abrupt increase of m_R corresponds to the transition from AP to P alignment of the magnetization [Fig. 9(b)]. The three lines plotted for the Ar and Ne ions as well as for Ga ions are very similar, making this dependence universal. Regardless of the type of ions and their energies, the same structural changes result in similar modifications of magnetic properties in the coupled Co/Mo/Co-layered structures.

V. SUMMARY: APPLICATION PERSPECTIVES

In this work, we present possibilities of magnetic property modifications of the Co/Mo/Co-layered structures by irradiation with 17-keV Ne, 30-keV Ar, and 35-keV Ga ions. The observed changes are compared and discussed as a function of the Mo spacer thickness and the ion fluence. The qualitative modifications observed with the beam fluence increase including: a decrease of the magnetic AP-coupling strength, a change of the coupling character from AP to P , conservation of the in-plane anisotropy easy-axis direction, and gradual suppression of the ferromagnetic behavior seem to be similar for all studied ion types. Quantitatively, the Ne ions are less effective—a higher fluence is necessary to obtain the same

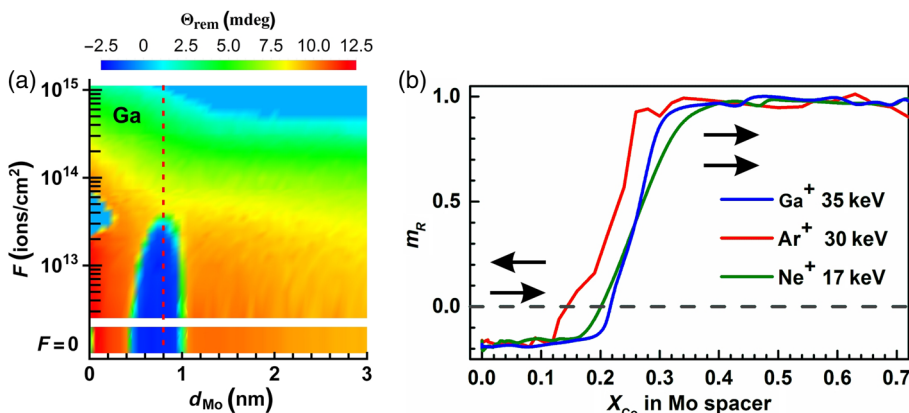


FIG. 9. (a) The map of $\theta_{\text{rem}}(d_{\text{Mo}}, F)$ measured along the EA after irradiation with 35-keV Ga ions. The vertical dashed line indicates the section along increasing F (related to X_{Co} in the Mo spacer) for $d_{\text{Mo}} = 0.8$ nm. (b) Cumulated for all ion types, the remanent normalized magnetization dependence on the Co concentration (in the center of the Mo spacer $d_{\text{Mo}} = 0.8$ nm marked by the arrow in Fig. 7) increasing with the ion fluence. The black arrows illustrate the magnetization alignment of the Co layers.

results as for the Ar or Ga ions. Magnetic modifications are explained satisfactorily by structural evolution estimated from the TRIDYN simulations.

The presented results are promising for the fabrication of periodic magnetic structures with desired modulated properties in the nanometer scale. This goal can be achieved by application of a focused ion beam or a combination of electron lithography and uniform irradiation with the parameters discussed in this work. It is expected that such structures will possess properties situating them in a group of magnonic crystals—a type of metamaterial that allows one to engineer band structure of spin waves. Such structures containing an ultrathin Co layer are currently the focus of great attention [53]. Very recently, the dynamics of magnetoelastic excitations in a one-dimensional magnonic phononic crystal consisting of alternating magnetic layers has been studied numerically [54]. Three examples of double-layer magnonic crystals are shown in Fig. 10. The irradiation of the Co/Mo/Co structures with AP coupling in an as-deposited state causes a local modification of the coupling resulting in oscillations between the AP and P alignment of magnetization [Fig. 10(a)]. In relatively low applied magnetic field $H > H_S$, magnetization can be switched to parallel, uniform orientation in both component Co layers [Fig. 10(b)]. In this way, a switchable magnonic crystal between patterned and magnetically uniform states can be obtained. In the P -coupled structures ($d_{\text{Mo}} > 1$ nm), irradiation can reduce locally magnetization saturation resulting in the spatial modulation of this parameter [Fig. 10(c)]. The application of high fluence may even quench ferromagnetism in the irradiated areas giving rise to modulations between magnetic and nonmagnetic states [Fig. 10(d)]. Higher fluence (than studied in this work) may

quench also the magnetization in the Co layers separated by the thin (e.g., $d_{\text{Mo}} = 0.8$ nm) Mo spacer. In this case, alternation between switchable AP-coupled and nonmagnetic states should be obtained. The patterned structures with nonmagnetic components are expected to be coupled by dipolar interactions. A desired type of modification can be easily achieved by the proper selection of the ion type and beam fluence. In-plane twofold anisotropy with preserved EA orientation after irradiation is another advantage of the Co/Mo/Co system. The direction of patterned stripes [Figs. 10(a), 10(c), and 10(d)] should be chosen along the EA. Such an orientation will additionally stabilize the magnetic patterned structure of magnonic crystals.

ACKNOWLEDGMENTS

This work is supported by the National Science Centre in Poland under the Project No. 2014/13/B/ST5/01834. Parts of this research are carried out at Ion Beam Centre at the Helmholtz-Zentrum Dresden—Rossendorf e. V., a member of the Helmholtz Association.

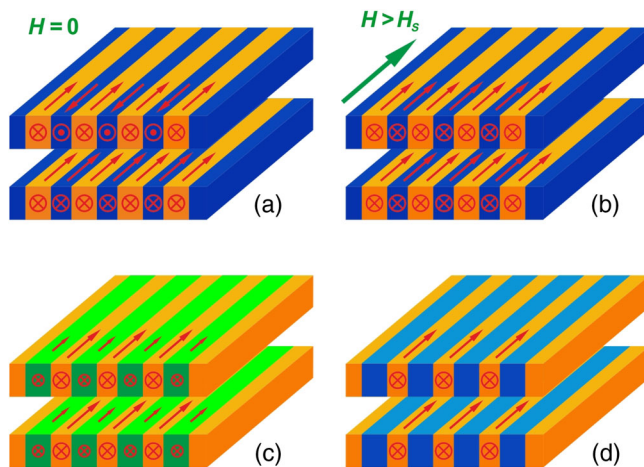


FIG. 10. An idea of various types of double-layer magnonic crystals in different magnetic states: (a), (b), (c), (d) that can be fabricated by local periodical irradiation with the ions and irradiation parameters discussed in this work (detailed description in the text). Magnetic states of the patterned structures are coded in the color scale of the maps from Fig. 3.

- [1] P. Grunberg, R. Schreiber, Y. Pang, M. B. Brodsky, and H. Sowers, Layered Magnetic Structures: Evidence for Antiferromagnetic Coupling of Fe Layers across Cr Interlayers, *Phys. Rev. Lett.* **57**, 2442 (1986).
- [2] C. Carbone and S.F. Alvarado, Antiparallel coupling between Fe layers separated by a Cr interlayer: Dependence of the magnetization on the film thickness, *Phys. Rev. B* **36**, 2433 (1987).
- [3] V. Grolier, D. Renard, B. Bartenlian, P. Beauvillain, C. Chappert, C. Dupas, J. Ferre, M. Galtier, E. Kolb, M. Mulloy, J. P. Renard, and P. Veillet, Unambiguous Evidence of Oscillatory Magnetic Coupling between Co Layers in Ultrahigh Vacuum Grown Co/Au(111)/Co Trilayers, *Phys. Rev. Lett.* **71**, 3023 (1993).
- [4] M. N. Baibich, J. M. Broto, A. Fert, F. Nguyen Van Dau, F. Petroff, P. Etienne, G. Creuzet, A. Friederich, and J. Chazelas, Giant Magnetoresistance of (001)Fe/(001)Cr Magnetic Superlattices, *Phys. Rev. Lett.* **61**, 2472 (1988).
- [5] R. E. Camley and J. Barnas, Theory of Giant Magnetoresistance Effects in Magnetic Layered Structures with Antiferromagnetic Coupling, *Phys. Rev. Lett.* **63**, 664 (1989).
- [6] M. Kisielewski, A. Maziewski, M. Tekielak, A. Wawro, and L. T. Baczewski, New Possibilities for Tuning Ultrathin Cobalt Film Magnetic Properties by a Noble Metal Overlayer, *Phys. Rev. Lett.* **89**, 087203 (2002).
- [7] S. Bandiera, R. C. Sousa, B. Rodmacq, and B. Dieny, Enhancement of perpendicular magnetic anisotropy through reduction of Co-Pt interdiffusion in (Co/Pt) multilayers, *Appl. Phys. Lett.* **100**, 142410 (2012).
- [8] C. Chappert, H. Bernas, J. Ferre, V. Kottler, J.-P. Jamet, Y. Chen, E. Cambril, T. Devolder, F. Rousseaux, V. Mathet, and H. Launois, Planar patterned magnetic media obtained by ion irradiation, *Science* **280**, 1919 (1998).
- [9] A. Maziewski, P. Mazalski, Z. Kurant, M. O. Liedke, J. McCord, J. Fassbender, J. Ferre, A. Mougin, A. Wawro,

- L. T. Baczewski, A. Rogalev, F. Wilhelm, and T. Gemming, Tailoring of magnetism in Pt/Co/Pt ultrathin films by ion irradiation, *Phys. Rev. B* **85**, 054427 (2012).
- [10] S. O. Demokritov, C. Bayer, S. Poppe, M. Rickart, J. Fassbender, B. Hillebrands, D. I. Kholin, N. M. Kreines, and O. M. Liedke, Control of Interlayer Exchange Coupling in Fe/Cr/Fe Trilayers by Ion Beam Irradiation, *Phys. Rev. Lett.* **90**, 097201 (2003).
- [11] V. E. Demidov, D. I. Kholin, S. O. Demokritov, B. Hillebrands, F. Wegelin, and J. Marien, Magnetic patterning of exchange-coupled multilayers, *Appl. Phys. Lett.* **84**, 2853 (2004).
- [12] S. Blomeier, B. Hillebrands, V. E. Demidov, S. O. Demokritov, B. Reuscher, A. Brodyanski, and M. Kopnarski, Magnetic patterning of Fe/CrFe(001) trilayers by Ga ion irradiation, *J. Appl. Phys.* **98**, 093503 (2005).
- [13] J. McCord, T. Strache, I. Monch, R. Mattheis, and J. Fassbender, Spatial manipulation of magnetic damping in ferromagnetic-antiferromagnetic films by ion irradiation, *Phys. Rev. B* **83**, 224407 (2011).
- [14] P. K. Greene, J. Osten, K. Lenz, J. Fassbender, C. Jenkins, E. Arenholz, T. Endo, N. Iwata, and K. Liu, Tuning perpendicular anisotropy gradient in Co/Pd multilayers by ion irradiation, *Appl. Phys. Lett.* **105**, 072401 (2014).
- [15] R. Bali, S. Wintz, F. Meutzner, R. Hübner, R. Boucher, A. A. Únal, S. Valencia, A. Neudert, K. Potzger, J. Bauch, F. Kronast, S. Facsko, J. Lindner, and J. Fassbender, Printing nearly-discrete magnetic patterns using chemical disorder induced ferromagnetism, *Nano Lett.* **14**, 435 (2014).
- [16] J. Fassbender and J. McCord, Magnetic patterning by means of ion irradiation and implantation, *J. Magn. Magn. Mater.* **320**, 579 (2008).
- [17] A. Aktag, S. Michalski, L. Yue, R. D. Kirby, and S. H. Liou, Formation of an anisotropy lattice in Co/Pt multilayers by direct laser interference patterning, *J. Appl. Phys.* **99**, 093901 (2006).
- [18] J. Kisielewski, W. Dobrogowski, Z. Kurant, A. Stupakiewicz, M. Tekielak, A. Kirilyuk, A. Kimel, Th. Rasing, L. T. Baczewski, A. Wawro, K. Balin, J. Szade, and A. Maziewski, Irreversible modification of magnetic properties of Pt/Co/Pt ultrathin films by femtosecond laser pulses, *J. Appl. Phys.* **115**, 053906 (2014).
- [19] I. Sveklo, Z. Kurant, A. Bartnik, D. Klinger, R. Sobierajski, A. Wawro, J. Kisielewski, M. Tekielak, and A. Maziewski, Modification of magnetic properties of Pt/Co/Pt trilayers driven by nanosecond pulses of extreme ultraviolet irradiation, *J. Phys. D* **50**, 025001 (2017).
- [20] J. B. Lee, G. G. An, S. M. Yang, H. S. Park, W. S. Chung, and J. P. Hong, Thermally robust perpendicular Co/Pd-based synthetic antiferromagnetic coupling enabled by a W capping or buffer layer, *Sci. Rep.* **6**, 21324 (2016).
- [21] O. Hellwig, T. L. Kirk, J. B. Kortright, A. Berger, and E. E. Fullerton, A new phase diagram for layered antiferromagnetic films, *Nat. Mater.* **2**, 112 (2003).
- [22] L. Fallarino, V. Sluka, B. Kardasz, M. Pinarbasi, A. Berger, and A. D. Kent, Interlayer exchange coupling between layers with perpendicular and easy-plane magnetic anisotropies, *Appl. Phys. Lett.* **109**, 082401 (2016).
- [23] F. Stobiecki, M. Urbaniak, B. Szymanski, J. Dubowik, P. Kuswik, M. Schmidt, T. Weis, D. Engel, D. Lengemann, A. Ehresmann, I. Sveklo, and A. Maziewski, Magnetic field induced transition from weak to strong ferromagnetic coupling in NiFe/Au/Co/Au multilayers, *Appl. Phys. Lett.* **92**, 012511 (2008).
- [24] J. H. Hsu, C. L. Tsai, C. M. Lee, and P. Saravanan, Modifying exchange-spring behavior of CoPt/NiFe bilayer by inserting a Pt or Ru spacer, *J. Appl. Phys.* **117**, 17A715 (2015).
- [25] M. Schafer, S. Demokritov, S. Muller-Pfeiffer, R. Schafer, M. Schneider, P. Grunberg, and W. Zinn, Investigation of 90° coupling in Fe/Ag/Fe structures: “Loose spins” and fluctuation mechanism, *J. Appl. Phys.* **77**, 6432 (1995).
- [26] R. R. Gareev, M. Buchmeier, M. Kiessling, G. Woltersdorf, and C. H. Back, Anomalous antiferromagnetic coupling in Fe/Si/Fe structures with Co “dusting”, *AIP Adv.* **1**, 042155 (2011).
- [27] T. Saerbeck, N. Loh, D. Lott, B. P. Toperverg, A. M. Mulders, A. Fraile Rodriguez, J. W. Freeland, M. Ali, B. J. Hickey, A. P. J. Stampfl, F. Klose, and R. L. Stamps, Spatial Fluctuations of Loose Spin Coupling in CuMn/Co Multilayer, *Phys. Rev. Lett.* **107**, 127201 (2011).
- [28] H. Yanagihara, H. Kamita, S. Honda, J. Inoue, E. Kita, H. Itoh, and K. Mibu, Antiferromagnetic coupling and impurity effects at junctions between Fe₃O₄ and Fe(001) layers, *Phys. Rev. B* **91**, 174423 (2015).
- [29] J. C. Slonczewski, Fluctuation Mechanism for Biquadratic Exchange Coupling in Magnetic Multilayers, *Phys. Rev. Lett.* **67**, 3172 (1991).
- [30] K. Schlage, L. Bocklage, D. Erb, J. Comfort, H. C. Wille, and R. Rohlsberger, Spin-structured multilayers: A new class of materials for precision spintronics, *Adv. Funct. Mater.* **26**, 7423 (2016).
- [31] W. K. Kuhn, J. W. He, and D. W. Goodman, IRAS study of CO adsorption on mixed Co and S overlayers on Mo(110), *J. Phys. Chem.* **98**, 264 (1994).
- [32] C. Morant, T. Campo, F. Marquez, C. Domingo, J. M. Sanz, and E. Elizalde, Mo-Co catalyst nanoparticles: Comparative study between TiN and Si surfaces for single-walled carbon nanotube growth, *Thin Solid Films* **520**, 5232 (2012).
- [33] K. Oikawa, G. W. Qin, M. Sato, O. Kitakami, Y. Shimada, J. Sato, K. Fukamichi, and K. Ishida, Magnetically induced phase separation and magnetic properties of Co-Mo hexagonal-close-packed structure thin films, *Appl. Phys. Lett.* **83**, 966 (2003).
- [34] C. Lin, G. W. Yang, and B. X. Liu, Different alloying behaviors of Co-Mo multilayered films upon ion irradiation and thermal annealing, *Appl. Phys. A* **70**, 469 (2000).
- [35] B. Zhao, G. H. Yang, F. Zeng, and F. Pan, Irradiation induced alloying and formation of amorphous films in Co-Mo system during ion beam assisted deposition, *Acta Mater.* **51**, 5093 (2003).
- [36] G. H. Yang, Y. Gu, Y. Gao, and F. Pan, Evolution of structure and magnetic properties from ferromagnetism to superparamagnetism in Co/Mo multilayers, *Thin Solid Films* **457**, 354 (2004).
- [37] G. H. Yang and F. Pan, Structural and magnetic properties of Co/Mo multilayers, *J. Magn. Magn. Mater.* **250**, 249 (2002).
- [38] N. Sato, Co-Mo thin films with an artificially layered structure, *J. Appl. Phys.* **63**, 3476 (1988).

- [39] Y. Wang, F.Z. Cui, W.Z. Li, and Y.D. Fan, Co/Mo multilayers deposited by ion-beam sputtering, *J. Magn. Mater.* **102**, 121 (1991).
- [40] C. Lin, Y. G. Chen, and B. X. Liu, Influence of annealing on the magnetic properties of alternate deposited Co/Mo thin film, *Thin Solid Films* **338**, 314 (1999).
- [41] J. Houserova, J. Vrestal, and M. Sob, Phase diagram calculations in the Co-Mo and Fe-Mo systems using first-principles results for the sigma phase, *Comput. Coupling Phase Diagrams Thermochem.* **29**, 133 (2005).
- [42] H. B. Guo, L. T. Kong, J. B. Liu, and B. X. Liu, *Ab initio* calculation to predict the possible nonequilibrium A_3B and AB_3 states in the Co-Mo system, *Solid State Commun.* **125**, 435 (2003).
- [43] S. S. P. Parkin, Systematic Variation of the Strength and Oscillation Period of Indirect Magnetic Exchange Coupling through the $3d$, $4d$, and $5d$ Transition Metals, *Phys. Rev. Lett.* **67**, 3598 (1991).
- [44] E. E. Shalyguina, E. V. Perepelova, L. Kozlovskii, and E. Tamanis, Magneto-optical investigation of Co/Mo/Co thin-film systems, *J. Magn. Mater.* **300**, e363 (2006).
- [45] D. D. Koelling, Magnetic multilayers with (Nb, Mo, Cr) spacer materials, *Phys. Rev. B* **50**, 273 (1994).
- [46] W. Moller, W. Eckstein, and J. P. Biersack, TRIDYN-binary collision simulation of atomic-collisions and dynamic composition changes in solids, *Comput. Phys. Commun.* **51**, 355 (1988).
- [47] M. Tikhov and E. Bauer, Growth, structure and energetics of ultrathin ferromagnetic single crystal films on Mo(110), *Surf. Sci.* **232**, 73 (1990).
- [48] J. Prokop, D. A. Valdaitsev, A. Kukunin, M. Pratzner, G. Schönhense, and H. J. Elmers, Strain-induced magnetic anisotropies in Co films on Mo(110), *Phys. Rev. B* **70**, 184423 (2004).
- [49] A. Mikkelsen, L. Ouattara, and E. Lundgren, Co on Mo(1 1 0) studied by scanning tunneling microscopy, *Surf. Sci.* **557**, 109 (2004).
- [50] A. Wawro, Z. Kurant, M. Tekielak, P. Nawrocki, E. Milińska, A. Pietruczik, M. Wójcik, P. Mazalski, J. Kanak, K. Ollefs, F. Wilhelm, A. Rogalev, and A. Maziewski, Engineering the magnetic anisotropy of an ultrathin Co layer sandwiched between films of Mo or Au, *J. Phys. D* **50**, 215004 (2017).
- [51] A. Wawro, Z. Kurant, M. Tekielak, M. Jakubowski, A. Pietruczik, R. Böttger, and A. Maziewski, Modifications of the magnetization ordering in Co/Mo/Co layers by Ga^+ ion irradiation, *Appl. Phys. Lett.* **110**, 252405 (2017).
- [52] Z. S. Shan, P. He, C. Moore, J. Woollam, and D. J. Sellmyer, Behavior of disordered Co-Pd, Co-Ag, and Co-Mo alloys in multilayer interfaces, *J. Appl. Phys.* **73**, 6057 (1993).
- [53] Q. Wang, A. V. Chumak, L. Jin, H. Zhang, B. Hillebrands, and Z. Zhong, Voltage-controlled nanoscale reconfigurable magnonic crystal, *Phys. Rev. B* **95**, 134433 (2017).
- [54] P. Graczyk, J. Klos, and M. Krawczyk, Broadband magnetoelastic coupling in magnonic-phononic crystals for high-frequency nanoscale spin-wave generation, *Phys. Rev. B* **95**, 104425 (2017).